



Identification of elastic property and loading fields from full-field displacement measurements

F. Amiot^{a,b,*} F. Hild^a J.P. Roger^b

^a*LMT Cachan, ENS de Cachan / CNRS-UMR 8535 / Université Paris 6*

61 avenue du Président Wilson, F-94235 Cachan Cedex, France.

^b*Laboratoire d'Optique Physique, ESPCI / CNRS-UPR A0005, 10 rue Vauquelin,*

F-75005 Paris, France.

Abstract

A method is introduced to identify simultaneously elastic properties and loading fields from a measured displacement field. Since the mechanical behavior of micro-electro-mechanical systems (MEMS) is governed by surface effects, this type of identification tool is thought to be of major interest. However, increasing the number of parameters to retrieve affects the redundancy necessary for an accurate identification. A finite-element formulation of a distance between measured and statically admissible (SA) displacement fields is shown to be equivalent to a standard least-squares distance to kinematically admissible (KA) fields if the used modeling is suitable. Any deviation from this equivalence is then the signature of a modeling error. Balancing the distance to KA and SA displacement fields allows one to retrieve unknown modeling parameters. This method is detailed on heterogeneous Euler-Bernoulli beams submitted to an unknown loading field and applied to experimental displacement fields of micro-cantilevers obtained with an electrostatic set-up. An elastic property field and a parameterized loading field are then identified, and the quality of the identification is assessed.

Key words: Identification problem, Full-field measurements, Cantilever, MEMS

* Corresponding author, amiot@lmt.ens-cachan.fr

Email addresses: amiot@lmt.ens-cachan.fr (F. Amiot),

hild@lmt.ens-cachan.fr (F. Hild), roger@optique.espci.fr (J.P. Roger).

1 Introduction

The increasing interest for micro-electro-mechanical systems (MEMS) has encouraged the development of many robust and accurate experimental techniques to deal with structures whose characteristic dimension lies within the 1-100 micrometer range (for a review, see Refs. [1–4]). These techniques may be divided into off-chip [5] and on-chip testing methods [6]. On the one hand, off-chip methods require to manipulate micrometer sized objects, and may become a challenging task. On the other hand, on-chip methods combine both micromachined specimen and actuation, and then require an accurate modeling of the whole device. Most of them involve a global kinematic measurement, translating at the micrometer scale some well known macroscopic set-ups [7]. A few of these techniques involve local displacement measurements [8], while full-field kinematic measurements are available at a macroscale [9]. More flexible actuation systems involve micro- and nano-indentation systems [10]. One of the main difficulty to perform full-field measurements at the micrometer scale is then the size of the set-up used to prescribe a mechanical point load. In general, a tip hides a large part of the field of view when the object is seen in reflection microscopy, creating an obstacle for local measurements. One way is to develop homogeneous tests at the microscale, where the observed area is different from the loading area [11]. Another way allowing for measurements is to use non-contact loading, namely by magnetic or electrostatic means. However, these techniques do not provide object-independent loadings, since the latter are subject to sharp edge effects. Consequently, heterogeneous tests require to identify both elastic property and loading fields.

Different techniques have been proposed to identify elastic properties using

redundant or full-field kinematic data. A first class is derived from the constitutive equation error, initially proposed in Refs. [12,13], applied to dynamic model updating [14] and elastic property or damage field identification [15]. It can also be used to deduce elastic properties by analyzing a heterogeneous test [16]. The virtual fields method represents another class, which has been used to identify homogeneous and anisotropic elastic properties of composites [17,18]. The reciprocity gap [19] is an alternative technique needing both kinematic and static quantities at the same location of the body boundary. It was used to identify elastic property fields or to locate cracks in elastic bodies [20]. Last, the elastic inversion [21] and the equilibrium gap methods [22] are both based on the equilibrium conditions written at the nodes of a finite-element model where the displacement is measured, both using the fact that there is no loading at the inner nodes of the structure. All these identification methods usually consist in retrieving a finite number of modeling parameters, resolving uniqueness issues [23], but requiring an a priori mechanical modeling of the test under consideration.

Since the MEMS behavior is driven by surface effects (*e.g.*, electrostatic, magnetic, chemical) whose homogeneity is very difficult to control, a method to identify both loading and elastic property fields from displacement fields is presented in Section 2. It is mainly based on a distance between measured and SA displacement fields, which is used to assess the identification quality. This distance to SA displacement fields is shown to be equivalent to a standard least-squares distance to KA fields, thus providing a modeling test, and thus allowing for the identification of modeling parameters. Compared to Lesnic [24], who demonstrated the difficulty of identifying the flexural rigidity field of a beam from deflection measurements using a continuum formulation, the case of

retrieving both flexural rigidity and loading fields of an Euler-Bernoulli beam is solved by using the described weak formulation of the problem and trying to minimize the equilibrium gap between elements. The main results and a sensitivity study to measurement noise are derived in Section 3. As the above mentioned methods, the present one is dependent on assumptions made on the elastic property fields and the loading field. If an assumption is not valid, this will yield an additional contribution to the residual equilibrium gap. This partition of the equilibrium gap is utilized to find a solution of the complete problem (*i.e.*, recovering both elastic property, and loading fields following an improved description of the structure under consideration) as both a distance to SA fields (related to the equilibrium gap) and KA fields. Last, the proposed procedure is applied to experimental data in Section 4.

2 Identification problem

Since the main objective of this work is to deal with structures experiencing a non-contact (*i.e.*, electrostatic, magnetic or chemical) loading, one has to identify both an elastic property field and a loading field from kinematic measurements. This contrasts with the above recalled methods, which are mainly devoted to the elastic property field identification for plane specimens loaded on a well-defined part of their boundaries.

2.1 Identification methods

2.1.1 Direct problem

Let us consider a solid body Ω . Each point M of Ω is located by \mathbf{x} . The material is assumed to be linear elastic, and the elastic property field $\mathcal{C}(\mathbf{x})$ is assumed to be known at each point \mathbf{x} of Ω . The boundaries of Ω may be decomposed such that:

- displacements $\mathbf{u}_d(M)$ are prescribed on S_u ;
- the stress vector $\mathbf{T}_d(M, \mathbf{n})$, where \mathbf{n} is orthogonal to the surface at the point M , is prescribed on S_t ;
- their intersection $S_u \cap S_t$ is usually not empty, and two cases should then be distinguished:
 - the mixed boundary conditions are not overlapping on $S_u \cap S_t$;
 - the boundary conditions result in an over-constrained set of equations.

Ω may also be submitted to a body-force distribution $\mathbf{f}(\mathbf{x})$. The local equilibrium conditions (static mode) read

$$\operatorname{div}(\sigma(\mathbf{x})) + \mathbf{f}(\mathbf{x}) = \mathbf{0} \quad (1)$$

where $\sigma(\mathbf{x})$ is the Cauchy stress tensor. On the boundary

$$\sigma(\mathbf{x})\mathbf{n} = \mathbf{T}_d \quad \forall \mathbf{x} \in S_t \quad (2)$$

One has to find the fields $(\mathbf{u}(\mathbf{x}), \sigma(\mathbf{x}))$ satisfying

$$\begin{aligned} \mathbf{u}(\mathbf{x}) &\in \mathcal{U}_{AD} \\ \sigma(\mathbf{x}) &\in \mathcal{S}_{AD} \end{aligned} \quad (3)$$

where

$$\mathcal{U}_{AD} = \left\{ \mathbf{u}(\mathbf{x}) \in H^1(\Omega) \mid \mathbf{u}(\mathbf{x}) = \mathbf{u}_d \quad \forall \mathbf{x} \in S_u \right\} \quad (4)$$

$$\mathcal{S}_{AD} = \left\{ \sigma(\mathbf{x}) \in H^1(\Omega) \mid \sigma(\mathbf{x})\mathbf{n} = \mathbf{T}_d \quad \forall \mathbf{x} \in S_t, \operatorname{div}(\sigma(\mathbf{x})) + \mathbf{f}(\mathbf{x}) = \mathbf{0} \quad \forall \mathbf{x} \in \Omega \right\} \quad (5)$$

and satisfying the constitutive equation

$$\sigma(\mathbf{x}) = \mathcal{C}(\mathbf{x})\epsilon[\mathbf{u}(\mathbf{x})] \quad \forall \mathbf{x} \in \Omega \quad (6)$$

In the small perturbations framework, the infinitesimal strain tensor reads

$$\epsilon(\mathbf{x}) = \frac{1}{2} [\nabla \mathbf{u}(\mathbf{x}) + \nabla \mathbf{u}^t(\mathbf{x})] \quad (7)$$

Except when the boundary conditions are over-constrained, one is able to prove the existence and uniqueness of a solution to the above problem, thus satisfying three different equation sets:

- kinematic conditions (4);
- equilibrium conditions (5);
- constitutive equation (6).

However, a few closed form solutions exist [25] and the direct problem has to be solved using variational principles. Satisfying both the virtual work principle and the constitutive equation error leads to the potential energy Δ_u of the structure

$$\forall \mathbf{u}_t \in \mathcal{U}_{AD} \quad \Delta_u(\mathbf{u}_t) = \frac{1}{2} \int_{\Omega} \epsilon[\mathbf{u}_t] : \mathcal{C} : \epsilon[\mathbf{u}_t] dV - \int_{\Omega} \mathbf{f} \cdot \mathbf{u}_t dV - \int_{S_t} \mathbf{T}_d \cdot \mathbf{u}_t dS \quad (8)$$

which has to be minimized with respect to the trial displacement field \mathbf{u}_t to provide an approximation to the solution of the direct problem, that is the displacement field \mathbf{u}_{sol} .

2.1.2 Inverse problem

The purpose of the identification problems is to retrieve some of mechanical parameters (known for the direct problem) from kinematic measurements, that is to find the description of a direct problem that would result in the measured displacement field. The available identification methods may use similar equation sets to retrieve the mechanical parameters under scrutiny, namely:

- kinematic conditions (4);
- equilibrium conditions (5);
- constitutive law (6).

Since the measurement noise corrupting the used displacement field is unavoidable, the above equation sets have to be over-determined to provide a reliable solution. To achieve this necessary redundancy, some assumptions are made to decrease the number of unknowns in the identification problem, thus increasing the inversion robustness wrt. the measurement noise. A global formulation of the identification problem is to find the displacement field \mathbf{U} minimizing φ^2

$$\varphi^2 = K_{KA}\|\mathbf{U} - \mathbf{U}_m\|_{KA} + K_{SA}\|\mathbf{U} - \mathbf{U}_{SA}\|_{SA} + K_{CE}\|\mathbf{U} - \mathbf{U}_{CE}\|_{CE} \quad (9)$$

that is matching “at best” the measured displacement field (*i.e.*, the kinematic conditions, first term), and satisfying equilibrium conditions (second term) as well as the constitutive law (third term). If the experimental information

is sufficient, various strategies, corresponding to different sets of the triplet (K_{KA}, K_{SA}, K_{CE}) and different minimization procedures, are then available. For example, finite-element updating methods [26] define the search space by enforcing the equilibrium equations and the constitutive law to be satisfied (in a weak form), and then intend to minimize φ^2 with $K_{SA} = K_{CE} = 0$. Alternatively, the methods primarily based on the use of equilibrium equations consist in minimizing φ^2 in a two-step process:

- the virtual fields method has been implemented using different kinds of measurement set-ups. The minimization of the first term is then performed to provide a projection of the displacement field on a suitable functions basis ($K_{KA} \neq 0$ and $K_{SA} = 0$). Afterwards, elastic properties are identified by satisfying the equilibrium equations obtained by using the constitutive equation in the virtual work principle ($K_{KA} = 0$ and $K_{SA} \neq 0$).
- the equilibrium gap method has been implemented with displacement fields obtained for digital image correlation measurements, that is after the minimization of a functional describing the optical flow conservation principle to find the expansion of the displacement field on a user-defined functional basis ($K_{KA} \neq 0$ and $K_{SA} = 0$). The mechanical parameters are then deduced by satisfying “at best” the equilibrium conditions at the nodes of the structure ($K_{KA} = 0$ and $K_{SA} \neq 0$).

The method based on the constitutive equation error presented in Ref. [15] consists also in minimizing φ^2 in a two-step process : the measured displacement field is first obtained with $K_{KA} \neq 0$ and $K_{SA} = K_{CE} = 0$. The mechanical parameters are then obtained by minimizing a chosen functional (proved to be separately convex with respect to the stress tensor and the elastic tensor), with $K_{CE} \neq 0$ and $K_{SA} = K_{KA} = 0$. A relaxation algorithm is then used

to exploit the separate convexity. The equilibrium conditions are enforced by defining the functional on SA stress fields.

In both cases, these two-step procedures highlight the major central compromise one has to deal with to save the equations redundancy and get reliable identified parameters, namely, one has to spatially average the measured quantities to reduce the effect of noise corrupting them, therefore having to balance this effect with the subsequent decrease in the independent measured quantities amount. Consequently, one has to deal with the mechanical counterpart of this unavoidable filtering process, by formulating the identification problem for discretized bodies.

2.2 *The equilibrium gap method*

The equilibrium gap method (EGM) has been primary formulated as this mechanical counterpart. Assuming the existence of a mesh of N_e elements describing the structure, a finite number of parameters, concatenated in the vector \mathbf{Q} , have to be identified. In the present case, the vector \mathbf{Q} may contain elastic, as well as loading parameters. Referring to Eq. (8), let us assume that the trial displacement field \mathbf{u}_t is expanded over a user-defined functions basis concatenated in the matrix \mathcal{M}_ϕ

$$\mathbf{u}_t = \mathcal{M}_\phi \mathbf{U} \quad (10)$$

where \mathbf{U} is vector of the nodal displacement field. The minimization conditions of the potential energy Δ_u read

$$\frac{\partial \Delta_u(\mathbf{Q}, \mathbf{U})}{\partial \mathbf{U}} = \mathbf{0} \quad (11)$$

Contrary to the resolution of the direct problem, the nodal displacement field \mathbf{U} is here considered as “almost” known (*i.e.*, measured)

$$\mathbf{U} \simeq \mathbf{U}_m \quad (12)$$

whereas the vector \mathbf{Q} is to be determined. Assuming that the elastic properties are piecewise homogeneous and that the inner nodes of the structure do not experience any external force, Claire et al. [22] obtained a system (11) of the form

$$\mathcal{M}\mathbf{Q} = \mathbf{0} \quad (13)$$

where the matrix \mathcal{M} depends upon the measured nodal displacements and the chosen shape functions $\phi_i(\mathbf{x})$. The above mentioned assumptions result in an over-determined linear system, which is found to provide reliable solutions even when the measured displacement field is submitted to significative noise levels. The solution \mathbf{Q}_{sol} does not exactly satisfy the system (13), and then one defines the residual \mathbf{F}_r

$$\mathcal{M}(\mathbf{U}_m)\mathbf{Q}_{sol} = \mathbf{F}_r \quad (14)$$

It is worth noting that this equilibrium equations match the standard form

$$\mathcal{M}(\mathbf{U}_m)\mathbf{Q}_{sol} = \mathcal{S}(\mathbf{Q}_{sol})\mathbf{U}_m - \mathbf{F}(\mathbf{Q}_{sol}) = \mathbf{F}_r \quad (15)$$

where \mathcal{S} is the identified stiffness matrix. If \mathbf{U}_m is SA, then the residual equilibrium gap is $\mathbf{F}_r = \mathbf{0}$. The projection \mathbf{U}_{SA} of the measured displacement field \mathbf{U}_m is then obtained (up to a rigid body motion) by solving

$$\mathcal{S}(\mathbf{Q}_{sol})\mathbf{U}_{SA} - \mathbf{F}(\mathbf{Q}_{sol}) = \mathbf{0} \quad (16)$$

Any norm of the residual \mathbf{F}_r then provides a distance between the measured displacement field and its projection \mathbf{U}_{SA} onto a statically admissible basis. However, this is no longer possible when the number of parameters to be identified (*i.e.*, the size of \mathbf{Q}) increases to reach the number of measured nodal displacements.

To overcome this limitation, let us note that since the problem is solved in the small perturbations framework, the behavior of the structure is assumed to be linear. If \mathbf{X} is a solution to system (13), then $h\mathbf{X}$ is a solution too $\forall h \in \mathbb{R}^*$. Consequently, a singular value decomposition of \mathcal{M} is used

$$\mathcal{M} = \mathcal{H}\mathcal{J}\mathcal{K}^t \quad (17)$$

where \mathcal{J} is a diagonal matrix, \mathcal{H} and \mathcal{K} are $N_u \times N_u$ orthogonal matrices in the considered limit case, where the number of parameters to retrieve is equal to the number of degrees of freedom. The diagonal elements of \mathcal{J} are the singular values of \mathcal{M} . The columns of \mathcal{K} (resp. \mathcal{H}) are the right (resp. left) singular vectors [27]. The non-trivial solution \mathbf{Q}_{sol} is proportional to the right singular vector associated with the least singular value of \mathcal{M} , which should be approximately equal to 0, within the machine precision. As a result, the solution is

$$\mathbf{Q}_{sol} = \vartheta \mathbf{k}_0 \quad (18)$$

where \mathbf{k}_0 is the column of \mathcal{K} (*i.e.*, the right singular vector) corresponding to the least singular value [27]. The sign of ϑ is prescribed by the constraint that the total strain energy of the structure E_s should be positive: $E_s > 0$. The mechanical loading and the elastic property fields are identified up to

a multiplicative constant (ϑ), since only kinematic data are considered. The results extracted from \mathbf{Q}_{sol} will then be referred to as loading and elastic property contrasts. If the singular value decomposition is performed with a high relative accuracy algorithm [28], it is possible to compute the residuals \mathbf{F}_r

$$\mathcal{M}\mathbf{k}_0 = \mathbf{F}_r \quad (19)$$

These residuals are a measure of the equilibrium gap and also local error estimators. To measure the quality of the identification, a global estimator W_r can be defined as the work of the residuals in the local displacement field $\mathbf{U}_{m\pm}$ (*i.e.*, the measured displacement field from which the rigid body motion of the two considered elements has been removed)

$$W_r = \sum_{i=1}^{N_u} |F_r(i)U_{m\pm}(i)| \quad (20)$$

Since this indicator includes the stress scale, this estimator needs to be compared to the total strain energy of the structure E_s

$$w_r = \frac{W_r}{E_s} \quad (21)$$

The estimator w_r is independent of the stress scale and evaluates the overall quality of the identification. It therefore enables for a measure of the distance between the measured displacement field and its projection onto a statically admissible basis, as defined by Eq. (15), and shown in Eq. (9). One may also compute the contribution of each element to the global indicator w_r , thus providing a local error indicator.

One may outline that using only the equilibrium conditions (13) in the present case, where the number of parameters to retrieve is equal to the number of measured kinematic parameters, would lead to a square linear system. This lack of redundancy would then yield a highly sensitive to noise solution. Therefore, as each condition is satisfied, it is no longer possible to get an error indicator, and then to assess the identification quality. The key point is then that assuming a linear behavior for the whole structure, one is then able to solve the identification problem and to associate an equilibrium gap to the solution, even if the number of parameters to retrieve (including both loading and elastic parameters) is equal to the number of measured nodal displacements. This improvement is of major interest to retrieve the most meaningful mechanical parameters from a measured (*i.e.*, corrupted) displacement field since it increases the number of parameters one can retrieve from a fixed number of kinematic parameters.

One can also note that this identification procedure may be corrupted by many different errors. One usually uses an idealized geometrical description, as well as one assumes a linear elastic material. Moreover, an idealized loading pattern as well as a too coarse discretization may induce additional errors. Since these errors result in non-satisfied stationarity conditions of the potential energy, they will induce an additional error gap. The next subsections are then devoted to the modeling improvement through the equilibrium gap minimization. The special case of a loading pattern error is detailed and the specificity of the latter error is emphasized.

2.3 Equivalence between static and kinematic criteria

Let us first consider that the modeling used to describe the structure is suitable. The aim of this section is then to assess the consequences of a noise corrupting the measured displacement field, resulting in a nodal displacement perturbation $\delta\mathbf{U}$. Thanks to the ideas proposed in Ref. [30], one is able to compute in a semi-analytical way the Jacobian of the singular value decomposition with respect to any parameter used to build the matrix \mathcal{M} . In particular, one is then able to compute the Jacobian of the equilibrium gap \mathbf{F}_r with respect to the displacement field \mathbf{U} from the singular value decomposition of \mathcal{M} (see Appendix A). One can also show that this Jacobian is described by a single non-singular vector \mathbf{U}_p near the solution, that is when the least singular value of \mathcal{M} is close to 0. The non-singular direction remains unique as long as the zero singular value of \mathcal{M} remains unique. This non-singular direction is also defined by

$$\mathbf{U}_p = \mathbf{H}_0^t \mathcal{S} \quad (22)$$

where \mathbf{H}_0 is the last column of \mathcal{H} and \mathcal{S} is the stiffness matrix of the structure (see Appendix B). As a consequence, if the nodal displacement field used to build the matrix \mathcal{M} is subjected to a perturbation $\delta\mathbf{U}$ orthogonal to the direction \mathbf{U}_p , the equilibrium gap is not significantly modified since the first order term is equal to 0

$$\mathbf{U}_p \cdot \delta\mathbf{U} = 0 \quad (23)$$

$$\frac{\partial \mathbf{F}_r}{\partial \mathbf{U}} \cdot \delta\mathbf{U} = \mathbf{0} \quad (24)$$

When computing the projection \mathbf{U} of the displacement field \mathbf{u} onto a kinematically admissible basis \mathcal{M}_ϕ , one usually minimizes the least-squares criterion

$$\|\mathbf{U} - \mathbf{U}_m\|_{KA} = v^2 = (\mathcal{M}_\phi \mathbf{U} - \mathbf{u})^t (\mathcal{M}_\phi \mathbf{U} - \mathbf{u}) \quad (25)$$

with respect to the trial displacement field \mathbf{U} . Let us then assume that the measured field $u(p)$ is subjected at point p to a Gaussian uncorrelated noise $b(p)$, with zero mean and σ^2 variance. Let us also recall that the modeling used to describe the structure is assumed to be suitable. It means that the discretization level is high enough to describe the measured displacement field, therefore only the noise defines the minimum value of v^2 (see Appendix C,a)

$$E[v_{min}^2] = \sigma^2 (N_p - N_u) \quad (26)$$

where $E[\cdot]$ denotes the expectation for the scalar \cdot , N_p the number of measurement points and N_u the number of nodal displacements in \mathbf{U} . v_{min}^2 is then a measure of the measurement noise.

As a consequence of the previous discussion on the non-singular direction \mathbf{U}_p , let us consider the projection of the displacement perturbation $\delta\mathbf{U}$ onto the non-singular direction \mathbf{U}_p , and denote κ the scalar

$$\kappa = \delta\mathbf{U}^t \mathbf{U}_p \quad (27)$$

The equilibrium gap \mathbf{F}_r is then proportional to the scalar κ . The expectation for the scalar κ^2 is found to be proportional to σ^2 , and the coefficient is found to depend on the used shape functions (see Appendix C,b). Therefore, the squared 2-norm of the equilibrium gap $\mathbf{F}_r^t \mathbf{F}_r$ is proportional to the noise level σ^2 if the used modeling is suitable, and the multiplicative constant between

them depends on both the stiffness matrix of the structure and the used shape functions. Dealing with load and elastic property contrasts, its range is obtained only from the used shape functions. The kinematic and static terms in Eq. (9) are then proportional to each other if the used modeling is suitable to the measured displacement field. Any deviation from this relationship provides a simple criterion to detect an unsuitable modeling, and this can be easily assessed if the noise level is experimentally known.

2.4 Modeling errors correction

Assuming that the used shape functions can describe the measured displacement field, the kinematic term in Eq. (9) arises only from the measurement noise. Under this assumption, the only way to depart from the above relationship between the kinematic and static term is to consider that a modeling error results in an additional contribution to the equilibrium gap. Assuming small perturbations, we consider an additive decomposition

$$\mathbf{F}_r = \mathbf{F}_{ru}(\delta\mathbf{U}_m^t \mathbf{U}_p) + \mathbf{F}_{rm} \quad (28)$$

where $\mathbf{F}_{ru}(\delta\mathbf{U}_m^t \mathbf{U}_p)$ is the contribution of the measurement noise $\delta\mathbf{U}_m = \mathbf{U}_m - \mathbf{u}_{sol}$ to the equilibrium gap, and \mathbf{F}_{rm} is the modeling error contribution. One should highlight that the partition (28) does not specify the origin of the additional modeling term \mathbf{F}_{rm} . Under the previous assumptions, this modeling error could arise from a wrong elastic property or loading pattern. The modeling errors due to a too coarse finite element model are not considered herein, since these discretization errors induce both an additional kinematic and static term in Eq. (9). One has also to provide another mechanical de-

scription to get a residual equilibrium gap matching the estimated noise level. This new mechanical model may be parameterized to compensate for the best modeling contribution to the equilibrium gap. Let us then consider the case of a single modeling parameter β , so that the equilibrium gap corresponding to the measured displacement field reads

$$\mathbf{F}_{\mathbf{r}}(\delta\mathbf{U}_m, \beta) = \mathbf{F}_{\mathbf{r}u}(\delta\mathbf{U}_m^t \mathbf{U}_p) + \mathbf{F}_{\mathbf{r}m}(\beta) \quad (29)$$

where $\delta\mathbf{U}_m$ is the displacement perturbation due to measurement uncertainties. The problem consists in looking for the β value that decreases the modeling contribution to the equilibrium gap.

Since only the total equilibrium gap $\mathbf{F}_{\mathbf{r}}(\delta\mathbf{U}_m, \beta)$ can be computed, one has to cancel out both terms in Eq. (29). From Appendix B, it can be inferred that near the solution, both contributions are proportional to the last column of the matrix \mathcal{H} . As a consequence, one obtains a 1D solution subspace, and one needs another information to decouple the contributions to the distance to a statically admissible field arising from the measurement noise and the modeling error, that is to find the correction displacement field $\delta\mathbf{U}_{sol} = -\delta\mathbf{U}_m$ and the solution modeling parameter β_{sol} so that

$$\mathbf{F}_{\mathbf{r}u}((\delta\mathbf{U}_m + \delta\mathbf{U}_{sol})^t \mathbf{U}_p) = \mathbf{0} \quad (30)$$

$$\mathbf{F}_{\mathbf{r}}(\delta\mathbf{U}_m + \delta\mathbf{U}_{sol}, \beta_{sol}) = \mathbf{0} \quad (31)$$

Only the projection of $\delta\mathbf{U}_m$ onto \mathbf{U}_p needs (and has) to be recovered. It is worth noting that the two above conditions state that the solution has to be both kinematically and statically admissible. This additional information (necessary to decouple the effects) is then naturally deduced from the noise level σ^2 , which is assumed to be known, either by the measurement assess-

ment or by the value of the distance from the measured displacement field to its projection onto a kinematically admissible basis (see Appendix C.a). According to Appendix C.b, the probability density for κ^2 is deduced from σ^2 and the used shape functions, thus providing a probability density of $\delta\mathbf{U}_{sol}$ satisfying Eq. (30) (*i.e.*, the kinematic condition). Using this probability density in Eq. (31) leads to restrict the solution space to a part of the above 1D solution space, and then provides a probability density for β_{sol} . If one considers both a displacement perturbation and N_m modeling parameters to be identified, the static admissibility provides a single relationship (31) and the kinematic admissibility provides a probability density, so that if $N_m > 1$, this information is useful to reduce the solution space but not sufficient to find a unique modeling parameters set.

3 Application to cantilever beams

Since the idea is valid for any structure, the above development is applied to beams of any size. A heterogeneous Euler-Bernoulli beam is discretized with N_e elements. Let α denote the discretization level of a beam by using $N_e = 2^\alpha$ elements. For instance, a cantilever beam is considered. The elastic property field is assumed to be heterogeneous, and is modeled with a (multiplicative) contrast field \mathbf{C} , where EIC_n is the flexural stiffness of the element n , $n \in \{1 \dots N_e\}$. The beam is only subjected to nodal forces \mathbf{F} , where F_m is the force applied on node m , $m \in \{1 \dots N_e\}$ (see Fig. 1). When the nodal forces and the stiffness field are known, the direct (classical) problem is to find the nodal displacement field $\mathbf{U} = (\mathbf{v}, \theta)$, where \mathbf{v} are the nodal out-of-plane displacements, and θ are the nodal cross-section rotations. The present aim is

to solve the identification problem, *i.e.*, when the nodal displacement field is almost known (since it is measured), to find the stiffness and load fields.

3.1 EGM for Euler-Bernoulli beams

One assumes that the user-defined scale α is able to describe the beam behavior. The available data are the nodal displacement field, that may be derived from a discrete displacement field, projecting it onto a kinematically admissible basis. The element length is ℓ . Following the equilibrium gap method [22], the equilibrium of each node is written as the stationarity of the potential energy

$$E_p = \frac{EI}{2} \sum_{n=1}^{N_e} C_n f(v_{n-1}, v_n, \theta_{n-1}, \theta_n) - \sum_{m=1}^{N_e} F_m v_m \quad (32)$$

where EI is the flexural stiffness, and

$$\begin{aligned} f(v_{n-1}, v_n, \theta_{n-1}, \theta_n) = & \frac{12}{\ell^3} (v_n - v_{n-1})^2 + \frac{4}{\ell} (\theta_n^2 + \theta_{n-1}^2 + \theta_{n-1} \theta_n) \\ & + \frac{12}{\ell^2} (v_{n-1} \theta_{n-1} + v_{n-1} \theta_n - v_n \theta_{n-1} - v_n \theta_n) \end{aligned} \quad (33)$$

It follows, for the n -th node, that

$$\begin{aligned} \frac{\partial E_{p_{n,n+1}}}{\partial v_i} &= \frac{EI}{2} \{C_n g^- + C_{n+1} g^+\} - F_i = 0 \\ \frac{\partial E_{p_{n,n+1}}}{\partial \theta_i} &= \frac{EI}{2} \{C_n h^- + C_{n+1} h^+\} = 0 \end{aligned} \quad (34)$$

with

$$\begin{aligned}
g^-(v_i, v_{i-1}, \theta_i, \theta_{i-1}) &= \frac{24}{\ell^3}(v_i - v_{i-1}) - \frac{12}{\ell^2}(\theta_{i-1} + \theta_i) \\
g^+(v_i, v_{i+1}, \theta_i, \theta_{i+1}) &= \frac{24}{\ell^3}(v_i - v_{i+1}) + \frac{12}{\ell^2}(\theta_i + \theta_{i+1}) \\
h^-(v_i, v_{i-1}, \theta_i, \theta_{i-1}) &= \frac{12}{\ell^2}(v_{i-1} - v_i) + \frac{4}{\ell}(\theta_{i-1} + 2\theta_i) \\
h^+(v_i, v_{i+1}, \theta_i, \theta_{i+1}) &= \frac{12}{\ell^2}(v_i - v_{i+1}) + \frac{4}{\ell}(2\theta_i + \theta_{i+1})
\end{aligned} \tag{35}$$

where \mathbf{v} and θ are the components of the measured nodal displacement field \mathbf{U}_m . In the present case, the field \mathbf{F} is unknown, in addition to the contrast field \mathbf{C} . The equilibrium conditions give $N_u = 2(N_e + 1)$ equations with $N_u = 2(N_e + 1)$ unknowns, which reduce to $2N_e$ independent equations with $2N_e$ unknowns if the first node is assumed to be motionless. At the α scale, the system of $2^{\alpha+1} + 2$ equations becomes

$$\mathcal{M}\mathbf{Q} = \mathbf{0} \tag{36}$$

with the unknown vector

$$\mathbf{Q}^t = [C_1, F_1, C_2, F_2, \dots, C_{2^{\alpha+1}}, F_{2^{\alpha+1}}] \tag{37}$$

where \mathcal{M} is a matrix that depends only on the measured nodal fields, which are obtained from the projection onto cubic Hermite functions (see Appendix D), on the assumed loading pattern and on the length of the element. $\mathbf{Q} = \mathbf{0}$ is the trivial solution. The solution \mathbf{Q}_{sol} is then obtained from the singular value decomposition (Eq. (17)), yielding the identified elastic and loading contrasts.

3.2 Static-kinematic equivalence for suitable models

The following results are all obtained with a beam discretized with 2^α elements. The flexural stiffness is homogeneous for each element, and the random contrast field follows a uniform probability density between 0.1 and 0.9 (Fig. 2). The mechanical loading is a homogeneous nodal force field. The displacement field \mathbf{u} is computed, and corrupted with a random white noise. To quantify the identification error on the sought fields, the error η on the the field \mathbf{Z} (with $\mathbf{Z} = \mathbf{C}$ or \mathbf{F}) is defined by

$$\eta(\mathbf{Z}) = \frac{1}{N_e} \sum_{k=1}^{N_e} \left(\frac{Z_{id}(k)}{Z_{imp}(k)} - 1 \right)^2 \quad (38)$$

The influence of a random white noise added to “FE” measurements on the identification quality is assessed. The results shown in Fig. 3a are averages over 100 realizations of white noise, with a prescribed noise/signal ratio. When the noise/signal ratio tends to zero, the identification error vanishes, thereby proving that the proposed procedure is correct. At a given discretization level, the identified load field is more sensitive to measurement noise than the elastic property field. These results also show the effect of discretization on the sensitivity to noise of the kinematically admissible fields. These simulations show an acceptable noise/signal ratio of almost 1% for 2 elements, which introduces an error of a few percents on the identified fields. This acceptable noise signal ratio decreases to 0.1% for 4 elements. All the results are summarized in Table 1. The estimator w_r is independent of the stress scale and evaluates the overall quality of the identification. This indicator is also related to the identification error η , as shown in Fig. 3b for the elastic property contrast. Identical results are obtained using the loading contrast, so that w_r is a global error

estimator to assess the identification results when the used model is suitable. The relationship between the identification error η and the estimator w_r is consistent with the results of Appendix C.b and is then single-valued, so that in the latter case, the quantity w_r is a measure of the identification error.

3.3 Modeling errors

In Section 3.2 the way in which the loading is applied on the structure is assumed to be well known, and is utilized to build the equilibrium matrix \mathcal{M} . In a practical case, full-field measurements provide enough information to allow for testing the chosen mechanical modeling, especially regarding the loading. This is tested on “FE” measurements, generated in the same way as in Section 3.2, but an additional nodal moment C_{end} proportional to the nodal forces F_{end} , is applied on the last node (see Fig. 1)

$$C_{end} = \beta_{sol} F_{end} \quad (39)$$

with $\beta_{sol} \neq 0$. The aim of this section is then to exhibit the consequences of an unknown loading pattern on the identification and to illustrate the proposed identification procedure to retrieve the loading pattern, *i.e.*, the unknown value for β .

3.3.1 Sensitivity of the equilibrium gap to the loading pattern

The partition (29) states that, close to the solution, the equilibrium gap depends on two scalar parameter. Thus, dealing with a single modeling parameter, one is able to plot a 2-D map of the norm of the equilibrium gap versus $\beta - \beta_{sol}$ and $\kappa = \delta \mathbf{U}^t \mathbf{U}_p$. Such a map, obtained with noisy computer-generated

displacement fields, is plotted in Fig. 4. One can note a deep and narrow valley, which corresponds to a zero-gradient direction in the (β, κ) plane. Let us denote by λ this zero-gradient direction, and λ_{\perp} the orthogonal one. Then, using the static criterion $\|\mathbf{F}_r\| = 0$ restricts the solution subspace to a single line, whose direction is λ , thereby proving that a static criterion is not sufficient to find a unique solution for β .

3.3.2 Kinematic noise criterion

To find a unique value for β , one has also to find the value of κ , where $\delta\mathbf{U}$ is the kinematically admissible projection of the true noise field \mathbf{b} corrupting the measured displacement field \mathbf{u} . If one makes the assumption that the measurement is shot-noise limited and that this noise is uncorrelated, one can derive an expression for the projection of this noise onto a kinematically admissible basis. Since the noise is assumed to be uncorrelated, the correlation coefficients between its projections onto the basis functions can be derived analytically and this allows one to compute the probability density for κ^2 (see Appendix B). This probability density defines a confidence region along the κ axis, in which the solution satisfying Eq. (30) should lie. Figure 5a shows the value of this criterion in the vicinity of the solution, and its complementarity to the equilibrium gap, when choosing a probability density to find the solution at a given point along the λ axis.

3.3.3 Combining both criteria

From the previous analyses, one is able to locate a confidence region in the (β, κ) plane when combining the static criterion $\|\mathbf{F}_r\| = 0$ (which sets the

position along the λ_{\perp} direction) and the computed probability density that defines a confidence region along the λ axis. Last, one gets a probability density for the parameter β (see Fig. 5b), which may be integrated to give error bounds.

4 Application to experimental results

4.1 Electrostatic loading

The set-up uses the fact that the present MEMS (Fig. 6a) is covered by a conducting gold layer, which can be utilized as an electrode of a capacitor. The other plate is a stamped aluminum sheet put almost 1 mm above the cantilevers. The parallelism between the two plates is adjusted thanks to visual inspection. As the air gap is quite big (1 mm), this provides a good enough parallelism. This plate has a 0.6 mm diameter hole, which allows one to observe the sample with a microscope (Fig. 7), since this hole is placed above the observed cantilever. If one prescribes a potential gap $V_1 - V_2$ between the armatures of a plane capacitor, an electric field $\mathbf{E}_f = -\nabla V$ appears. Each plate yields a surface charge $\pm\sigma_q$ defined by

$$\sigma_q = E_f \varepsilon_e \quad (40)$$

where ε_e is the dielectric constant of the medium. The armatures will attract each other, independently of the sign of $(V_1 - V_2)$. This displacement will not significantly modify the electric field itself until it remains small compared with the gap between the armatures. For a small surface element dS , the force

dF applied to it is given by

$$dF = \frac{\sigma_q^2}{2\varepsilon_e} dS \quad (41)$$

Since the MEMS surface is an equipotential, the electric field and the force dF are orthogonal to the surface. Consequently, this mechanical loading can be described by a pressure field

$$p = \frac{\sigma_q^2}{2\varepsilon_e} \quad (42)$$

However, the used capacitor does not lead to a homogeneous electric field between the armatures since the upper one has a hole, and the lower one has many edges. Consequently, one cannot make any assumption concerning the homogeneity of the applied pressure field.

4.2 Retrieving the flexural rigidity and the electrostatic pressure field

The described algorithms, validated analytically and by using “FE” measurements, are now applied to fields obtained experimentally with the set-up described in Fig 7. The unknowns are the multiplicative contrast parameters and the pressure applied to each element, which is assumed to be constant along the element (see Fig. 8, $\beta = 0$). The displacement field is obtained through an interferometric imaging set-up. A typical measured optical phase field is shown in Fig. 9. Measuring such an optical phase field before and after applying a mechanical (electrostatic) loading allows one to compute the displacement field of the cantilever [29]. This displacement field is then averaged across the cantilever width to provide a one-dimensional displacement field. These fields are obtained under conditions that ensure a reproducibility

of almost 100 pm. The noise corrupting the measured displacement field is proven to be spatially uncorrelated [29], thus consistent with the assumptions of Appendix C. The field of view covers the whole cantilever and a part of the substrate. As shown in Fig. 3a, the noise/signal ratio limits the discretization level. Since maximum displacements, obtained under a 800 V potential gap, are of the order of 30 nm, a 2-element discretization is the maximum value for the present algorithm. The signal-noise ratio is of the order of one percent. One would expect a value of w_r in the 10^{-2} range (see Figs. 3a and 3b) if the used model is suitable. Figure 11b shows the scaled identified fields when assuming that the cantilever is subjected only to a pressure field. One can note a repulsive pressure near the clamped part of the cantilever, and the value of w_r reaches 2.8, thereby proving the poor quality of the identification results. Since it is quite different from the expected value (Fig. 3), one can assume a modeling error.

When looking at the measured displacement field in Fig. 11a, one can see a change in the cantilever curvature near its free end. Consequently one can assume that unexpected effects are not fully described with the chosen model. This is also confirmed when looking at the local contributions to w_r (Fig. 10a), which shows that an error arises at the free end of the cantilever. This poor identification result is confirmed by comparing the measured displacement field and the best SA displacement field obtained when $\beta = 0$ (the rigid body motion is chosen to minimize $\|\mathbf{U}_{SA} - \mathbf{U}_m\|_{KA}$). The difference between these fields is shown in Fig. 10b. A way of improving the solution is to consider that the electrostatic pressure applies to all the metallic faces of the gold layer on top of the cantilever, so that the pressure on the end surface will lead to an extra couple acting at the end of the cantilever (Fig. 8). This moment is

modeled by a dimensionless parameter β , which is the ratio between the nodal couple due to the pressure field arising on the last element and this additional parameter. Considering a single loading level, this assumption does not result in an extra relationship between loading parameters. This argument illustrates the fact that the proposed method is not intended to give the physical origin of the modeling error, but to identify a parameterized modeling frame and assess its quality with respect to a displacement field.

4.3 Retrieving the β ratio

The problem is to identify the best value for β . To solve this problem, a 3-step algorithm derived from the discussion of Section 3.3 is used:

- find a rough estimate β_0 , as the minimizer of $\|\mathbf{F}_{rm}\|$ with respect to β , using the measured displacement field,
- using the computed Jacobian and a Newton-Raphson algorithm, move down the valley of the static criterion,
- define the λ direction, and compute the probability density arising from the kinematic criterion along it. Projecting this confidence region onto the β axis returns a probability density for β .

Table 2 shows the resulting values for β , and Fig. 12 displays the final probability density for β . When integrating it, one can show for example that $P[-1.53 < \beta < -1.38] = 0.9$. Considering only the modeling correction, one gets (Table 2) a w_r value in the expected 10^{-2} range throughout the confidence interval, thereby proving the correction quality. When choosing a particular point in the defined confidence region, one can get some new identified fields,

which are shown (scaled) in Fig. 11. The pressure field is then attractive everywhere along the cantilever, which is consistent with what is expected. The flexural stiffness is found to increase near the motionless part of the cantilever. This extra stiffness may be explained by a remaining base under the cantilever, as a consequence of a silica underetching. This base is partially found on oblique SEM views of the beam (Fig. 6b). The identification quality is improved by comparing the corresponding SA and measured displacement fields (Fig. 13). The agreement also proves that a few, but rich elements are sufficient to describe complex and highly heterogeneous effects, provided that a rich modeling can be identified.

If one wants to perform the whole identification procedure with 4 elements, one should first note that the noise level is too high to get accurate identified fields (see Fig. 3a). The value of w_r reaches 11.7, and the identified stiffness fields present several negative values, thereby proving the poor quality of the identification. In this case, the minimization procedure fails to improve the estimated value $\beta_0 = -4.21$, corresponding to a value of w_r equal to 0.5.

5 Conclusion

An identification procedure is proposed to retrieve both heterogeneous stiffness and loading fields using full-field displacement measurements. This technique is based on local equilibrium conditions, thus defining a distance from the measured field to a statically admissible one, assuming some modeling hypothesis, even if the conditions redundancy is significantly affected by an increased number of parameters to be identified. Analytical derivations, as well as numerical simulations have been carried out to control the effect of an

additive white noise on the identified fields at different discretization levels, when the modeling hypotheses are satisfied.

Then, a significant gap between the computed value of the estimator and the expected one is studied as the consequence of a modeling error. Since it is a key point in the identification process, a strategy is developed to deal with modeling errors and to retrieve the unknown modeling parameter, when satisfying both static and (statistical) kinematic criteria.

Last, this procedure was applied to experimental results, providing stiffness and loading contrasts, and a statistical description of an a priori unknown modeling parameter, from full-field measurements on a MEMS. Since it is possible to deal with modeling errors, future analyses will consider the special case of a discretization error, in order to improve the spatial resolution of the identified properties.

Appendix A: Computing the Jacobian of the singular value decomposition

The key ideas of the following derivations were proposed in Ref. [30]. Using the definition of Eq. (17), one has to compute the Jacobian $\mathbf{D}_p = \frac{\partial \mathcal{M}}{\partial p}$ where p stands for a parameter used to build \mathcal{M} (*i.e.*, a component of the displacement field or the loading field). Let us recall that \mathcal{J} is diagonal, and that both \mathcal{H} and \mathcal{K} are orthogonal $N_u \times N_u$ matrices. \mathcal{J} is organized so that the singular values are sorted in decreasing order with respect to the indices. Taking the derivative of Eq. (17) with respect to p yields

$$\frac{\partial \mathcal{M}}{\partial p} = \frac{\partial \mathcal{H}}{\partial p} \mathcal{J} \mathcal{K}^t + \mathcal{H} \frac{\partial \mathcal{J}}{\partial p} \mathcal{K}^t + \mathcal{H} \mathcal{J} \frac{\partial \mathcal{K}^t}{\partial p} \quad (43)$$

Let us define \mathcal{M}_p as $\frac{\partial \mathcal{M}}{\partial p}$. Moreover, the orthogonality condition reads

$$\mathcal{H}^t \mathcal{H} = \mathcal{I} \quad (44)$$

$$\mathcal{K}^t \mathcal{K} = \mathcal{I} \quad (45)$$

where \mathcal{I} is the identity matrix. By derivation, one gets

$$\frac{\partial \mathcal{H}^t}{\partial p} \mathcal{H} + \mathcal{H}^t \frac{\partial \mathcal{H}}{\partial p} = (\Omega_H^p)^t + \Omega_H^p = 0 \quad (46)$$

$$\frac{\partial \mathcal{K}^t}{\partial p} \mathcal{K} + \mathcal{K}^t \frac{\partial \mathcal{K}}{\partial p} = (\Omega_K^p)^t + \Omega_K^p = 0 \quad (47)$$

where Ω_H^p and Ω_K^p are antisymmetric matrices

$$\Omega_H^p = \mathcal{H}^t \frac{\partial \mathcal{H}}{\partial p} \quad (48)$$

$$\Omega_K^p = \frac{\partial \mathcal{K}^t}{\partial p} \mathcal{K} \quad (49)$$

so that

$$\mathcal{H}^t \mathcal{M}_p \mathcal{K} = \Omega_H^p \mathcal{J} + \frac{\partial \mathcal{J}}{\partial p} + \mathcal{J} \Omega_K^p \quad (50)$$

Let us write \mathcal{M}_p

$$\mathcal{M}_p = \sum_{i,j=1}^{N_\alpha} \alpha_{pij} \mathbf{e}_i \otimes \mathbf{e}_j \quad (51)$$

where N_α is the number of terms involved in \mathcal{M}_p . Since Ω_H^p and Ω_K^p are antisymmetric matrices, and recalling that \mathcal{J} is diagonal, the diagonal elements of $\Omega_H^p \mathcal{J}$ and $\mathcal{J} \Omega_K^p$ are also vanishing, thereby yielding the derivatives of the singular values with respect to p

$$\frac{\partial J_{rr}}{\partial p} = \sum_{i,j=1}^{N_\alpha} \alpha_{pij} H_{ir} K_{jr} \quad (52)$$

Taking into account the antisymmetry property, the elements of the matrices Ω_H^p and Ω_K^p are computed by solving a set of linear systems, which are derived from the off-diagonal elements of the matrices in Eq. (50)

$$J_{ss} \Omega_{Hrs}^p + J_{rr} \Omega_{Krs}^p = \sum_{i,j=1}^{N_\alpha} \alpha_{pij} H_{ir} K_{js} \quad (53)$$

$$J_{rr} \Omega_{Hrs}^p + J_{ss} \Omega_{Krs}^p = - \sum_{i,j=1}^{N_\alpha} \alpha_{pij} H_{is} K_{jr} \quad (54)$$

This system has a unique solution provided $J_{ss} \neq J_{rr}$ for $s \neq r$, that is if the singular value decomposition has a unique solution. Once Ω_H^p and Ω_K^p have been computed, one can obtain

$$\mathbf{D}_p = \frac{\partial \mathcal{K}}{\partial p} = -\mathcal{K} \Omega_K^p \quad (55)$$

which is the desired derivative. The derivative with respect to the displacement field is then easily derived as the concatenation of the derivatives with respect to each nodal displacement. It is then possible to derive in a semi-analytical way the Jacobian of the equilibrium gap (14)

$$\frac{\partial \mathbf{F}_r}{\partial \mathbf{U}} = \frac{\partial \mathcal{M}}{\partial \mathbf{U}} \mathbf{Q} + \mathcal{M} \frac{\partial \mathbf{Q}}{\partial \mathbf{U}} \quad (56)$$

Noting that the first term is the identified stiffness matrix \mathcal{S} (see Eq. (15))

$$\frac{\partial \mathcal{M}}{\partial \mathbf{U}} \mathbf{Q} = \mathcal{S} \quad (57)$$

the Jacobian of the equilibrium gap reads

$$\frac{\partial \mathbf{F}_r}{\partial \mathbf{U}} = \mathcal{S} + \mathcal{M} \frac{\partial \mathbf{Q}}{\partial \mathbf{U}} \quad (58)$$

Since \mathbf{Q} is proportional to the last column of \mathcal{K} , the Jacobian of the equilibrium gap is obtained in a semi-analytical way from the SVD of \mathcal{M} .

Appendix B: Equilibrium gap Jacobian singularity near the solution

At the solution, the least singular value is zero

$$J_{NN} = 0 \quad (59)$$

where N stands for N_u to avoid multiple subscript. The linear system (53) becomes

$$J_{tt} \Omega_{KtN}^p = \sum_{i,j=1}^{N_\alpha} \alpha_{pij} H_{it} K_{jN} \quad (60)$$

noting that the stiffness matrix is related to the solution by (see Eq. (57))

$$S_{ip} = \sum_{j=1}^{N_\alpha} \alpha_{pij} K_{jN} \quad (61)$$

and Eq. (60) is replaced by

$$\Omega_{KtN}^p = \frac{1}{J_{tt}} \sum_{l=1}^{N_\alpha} H_{lt} S_{lp} \quad (62)$$

Comparing to Eq. (48), one is able to compute the gradient

$$\frac{\partial K_{rN}}{\partial p} = - \sum_{t=1}^{N_\alpha-1} K_{rt} \Omega_{KtN}^p \quad (63)$$

and then the Jacobian

$$\begin{aligned} \left. \frac{\partial \mathbf{F}_r}{\partial \mathbf{U}} \right|_i &= S_{ip} + \sum_{r=1}^{N_\alpha} M_{ir} \frac{\partial K_{rN}}{\partial \mathbf{U}} \\ &= S_{ip} - \sum_{l=1}^{N_\alpha} S_{lp} \sum_{r=1}^N M_{ir} L_{rl} \end{aligned} \quad (64)$$

with

$$L_{rl} = \sum_{t=1}^{N-1} \frac{K_{rt} H_{lt}}{J_{tt}} \quad (65)$$

so that \mathcal{L} corresponds to the definition of the pseudo-inverse of \mathcal{M}

$$\mathcal{L} = \mathcal{K} \mathcal{J}^* \mathcal{H}^t \quad (66)$$

where \mathcal{J}^* is deduced from \mathcal{J}

$$J_{kk}^* = \begin{cases} \frac{1}{J_{kk}} & \text{if } J_{kk} > 0 \\ 0 & \text{otherwise} \end{cases}$$

The condition $J_{NN} = 0$ implies that

$$\sum_{r=1}^N M_{ir} L_{rl} = \sum_{q=1}^{N-1} H_{iq} H_{lq} = \sum_{q=1}^N H_{iq} H_{lq} - H_{iN} H_{lN} = \delta_{il} - H_{iN} H_{lN} \quad (67)$$

where δ_{il} is the Kronecker symbol. Equation (64) can be rewritten as

$$\left. \frac{\partial \mathbf{F}_r}{\partial \mathbf{U}} \right|_i = \left(\sum_{l=1}^{N_\alpha} S_{lp} H_{lN} \right) H_{iN} \quad (68)$$

Close to the solution, the equilibrium gap arising from a measurement noise is then proportional to the last column of \mathcal{H} . One should underline that this last result is still valid when considering the equilibrium gap induced by the modification of any parameter p close to the solution. Let us denote the latter by \mathbf{H}_0 and \mathbf{U}_p the direction defined by

$$\mathbf{U}_p = \mathbf{H}_0^t \mathcal{S} \quad (69)$$

the Jacobian finally reads

$$\frac{\partial \mathbf{F}_r}{\partial \mathbf{U}} = \mathbf{H}_0 \otimes \mathbf{U}_p \quad (70)$$

As a consequence, the residuals are not modified if the nodal displacement field used to build the matrix \mathcal{M} is subjected to a perturbation $\delta \mathbf{U}$ orthogonal to the direction \mathbf{U}_p

$$\mathbf{U}_p \cdot \delta \mathbf{U} = 0 \quad (71)$$

$$\frac{\partial \mathbf{F}_r}{\partial \mathbf{U}} \cdot \delta \mathbf{U} = \mathbf{0} \quad (72)$$

where \mathbf{U}_p is then the single non-singular direction of the Jacobian $\frac{\partial \mathbf{F}_r}{\partial \mathbf{U}}$. This non-singular direction remains unique as long as the zero singular value of \mathcal{M} remains unique.

Appendix C: Definition of the kinematic noise criterion

One assumes that the measured field $u(p)$ is subjected at point p to a Gaussian uncorrelated noise $b(p)$, with zero mean and σ^2 variance.

a Projection onto a kinematically admissible basis

When computing the projection of the displacement field onto a kinematically admissible basis, one minimizes the scalar

$$v^2 = (\mathcal{M}_\phi \mathbf{U} - \mathbf{u})^t (\mathcal{M}_\phi \mathbf{U} - \mathbf{u}) \quad (73)$$

where \mathcal{M}_ϕ is the interpolation matrix, \mathbf{U} the sought (nodal) displacement field, and \mathbf{u} the measured one. The stationarity condition reads

$$\mathcal{M}_\phi^t \mathcal{M}_\phi \mathbf{U}_m = \mathcal{M}_\phi^t \mathbf{u} \quad (74)$$

When \mathbf{u} is subjected to measurement noise, it reads

$$\mathbf{u} = \mathbf{u}_0 + \mathbf{b} \quad (75)$$

where \mathbf{u}_0 is the true displacement field. The corresponding partition on the obtained displacement field becomes

$$\mathbf{U}_m = \mathbf{U}_0 + \delta \mathbf{U} \quad (76)$$

with

$$\mathcal{M}_\phi \mathbf{U}_0 = \mathbf{u}_0 \quad (77)$$

so that

$$\mathcal{M}_\phi^t \mathcal{M}_\phi \delta \mathbf{U} = \mathcal{M}_\phi^t \mathbf{b} \quad (78)$$

and the minimum value of v^2 , v_{min}^2 reads

$$v_{min}^2 = \mathbf{b}^t \mathbf{b} - \delta \mathbf{U}^t \mathcal{Y} \delta \mathbf{U} \quad (79)$$

with $\mathcal{Y} = \mathcal{M}_\phi^t \mathcal{M}_\phi$. Then

$$E[v_{min}^2] = E[\mathbf{b}^t \mathbf{b}] - E[\delta \mathbf{U}^t \mathcal{Y} \delta \mathbf{U}] \quad (80)$$

where $E[\cdot]$ denotes the expectation for the scalar \cdot . If N_p is the number of independent measurement points, $E[\mathbf{b}^t \mathbf{b}] = N_p \sigma^2$ and

$$E[\delta \mathbf{U}^t \mathcal{Y} \delta \mathbf{U}] = E[\mathbf{b}^t \mathcal{M}_\phi \mathcal{Y}^{-1} \mathcal{M}_\phi^t \mathbf{b}] \quad (81)$$

When $\mathbf{X} = \mathcal{M}_\phi^t \mathbf{b}$, the previous quantity becomes,

$$E[\delta \mathbf{U}^t \mathcal{Y} \delta \mathbf{U}] = \sum_{i,j} \mathcal{Y}_{ij}^{-1} E[X_i X_j] \quad (82)$$

Following its definition,

$$X_i = \sum_{n=1}^{n=N_\alpha} \phi_i(n) b(n) = \sum_{n=1}^{n=N_\alpha} x_i(n) = \langle \phi_i, b \rangle \quad (83)$$

where $\phi_i(n)$ is a shape function, that is the i -th column of \mathcal{M}_ϕ . If the $b(n)$ components are uncorrelated, the covariance is obtained as a function of the

shape functions

$$\begin{aligned}
E[X_i X_j] &= \sum_{n=1}^{N_\alpha} E[x_i(n) x_j(n)] \\
&= \sum_{n=1}^{N_\alpha} \int_{-\infty}^{\infty} \phi_i(n) \phi_j(n) \frac{x^2}{\sigma\sqrt{2\pi}} \exp\left(-\frac{x^2}{2\sigma^2}\right) dx \\
&= \sigma^2 \langle \phi_i, \phi_j \rangle \\
&= \sigma^2 \mathcal{Y}_{ij}
\end{aligned} \tag{84}$$

Then,

$$E[v_{min}^2] = \sigma^2 (N_\alpha - \mathcal{Y}^{-1} : \mathcal{Y}) = \sigma^2 (N_p - N_u) \tag{85}$$

where N_u is the number of nodal displacements in \mathbf{U} . Thus, when the chosen discretization level is suitable to describe the displacement field, the value of v_{min}^2 is a measure of the noise level.

b Application to the partition of the projection of a measurement noise onto a kinematically admissible basis

As explained in Section 3.3.2, the displacement perturbation reads

$$\delta \mathbf{U} = \kappa \mathbf{U}_p + \mathcal{W} \mathbf{s} \tag{86}$$

Since \mathbf{U}_p and the columns of \mathcal{W} are obtained from the right singular vectors of $\frac{\partial \mathbf{F}_r}{\partial \mathbf{U}}$, their concatenation yields an orthogonal basis for the kinematically admissible displacement fields, so that

$$\mathcal{W}^t \mathbf{U}_p = \mathbf{0} \tag{87}$$

$$\mathcal{W}^t \mathcal{W} = \mathcal{I} \quad (88)$$

$$\mathbf{U}_p^t \mathbf{U}_p = 1 \quad (89)$$

The minimization of v^2 (see Eq. (73)) yields

$$A\kappa = \mathbf{U}_p^t \mathcal{M}_\phi^t \mathbf{b} - \mathbf{U}_p^t \mathcal{Y} \mathcal{W} \mathcal{D}^{-1} \mathcal{W}^t \mathcal{M}_\phi^t \quad (90)$$

when using the following notations

$$A = \mathbf{U}_p^t \mathcal{Y} \mathbf{U}_p - \mathbf{U}_p^t \mathcal{Y} \mathcal{W} \mathcal{D}^{-1} \mathcal{W}^t \mathcal{Y} \mathbf{U}_p \quad (91)$$

$$\mathcal{D} = \mathcal{W}^t \mathcal{Y}^t \mathcal{W} \quad (92)$$

Moreover, the displacement partition (86) implies that

$$\delta \mathbf{U}^t \delta \mathbf{U} = B\kappa^2 - \frac{2}{A} \mathbf{b}^t \mathcal{M}_\phi \mathcal{F} \mathcal{M}_\phi^t \mathbf{b} \quad (93)$$

with

$$B = 1 + \mathbf{U}_p^t \mathcal{Y} \mathcal{T} \mathcal{Y} \mathbf{U}_p \quad (94)$$

$$\mathcal{T} = \mathcal{W} \mathcal{D}^{-1} \mathcal{W}^t \mathcal{W} \mathcal{D}^{-1} \mathcal{W}^t \quad (95)$$

$$\mathcal{F} = \mathbf{U}_p \mathbf{U}_p^t \mathcal{Y} \mathcal{T} - \mathcal{W} \mathcal{D}^{-1} \mathcal{W}^t \mathcal{Y} \mathbf{U}_p \mathbf{U}_p^t \mathcal{Y} \mathcal{T} + \mathcal{T} \quad (96)$$

Then, the expectation of κ^2 reads

$$E[\kappa^2] = \frac{\sigma^2}{B} \left(\mathcal{Y}^{-1} \mathcal{Y}^{-1} + \frac{2}{A} \mathcal{F} \right) : \mathcal{Y} \quad (97)$$

$$= \sigma_\kappa^2$$

and the sought quantity becomes,

$$\begin{aligned} E[(\kappa^2 - E[\kappa^2])^2] &= \int_{-\infty}^{\infty} \frac{x^4}{\sigma_\kappa \sqrt{2\pi}} \exp\left(-\frac{x^2}{2\sigma_\kappa^2}\right) dx - \sigma_\kappa^4 \\ &= 2\sigma_\kappa^4 \end{aligned} \quad (98)$$

Appendix D: Shape functions

Figure 14 describes the used nodal displacements to represent the the deformation of an element of length ℓ . The out-of-plane displacement is denoted v , and the cross-section rotation is denoted θ . The out-of-plane displacement field is described by a cubic polynomial, whose coefficients are expressed as a function of the nodal displacements thanks to the Euler-Bernoulli hypothesis

$$\theta(y) \simeq \frac{\partial v(y)}{\partial y} \quad (99)$$

The displacements field then reads

$$\begin{bmatrix} v(y) \\ \theta(y) \end{bmatrix} = \begin{bmatrix} 1 - 3\tilde{y}^2 + 2\tilde{y}^3 & \ell(\tilde{y} - 2\tilde{y}^2 + \tilde{y}^3) & (3\tilde{y}^2 - 2\tilde{y}^3) & \ell(\tilde{y}^3 - \tilde{y}^2) \\ \frac{6}{\ell}(\tilde{y}^2 - \tilde{y}) & (3\tilde{y}^2 - 4\tilde{y} + 1) & -\frac{6}{\ell}(\tilde{y}^2 - \tilde{y}) & (3\tilde{y}^2 - 2\tilde{y}) \end{bmatrix} \begin{bmatrix} v_1 \\ \theta_1 \\ v_2 \\ \theta_2 \end{bmatrix} \quad (100)$$

where

$$\tilde{y} = \frac{y}{\ell} \quad (101)$$

The strain energy reads, after neglecting the shear terms

$$E_s = \frac{1}{2} \int_{y=0}^{y=\ell} EI \left(\frac{\partial^2 v}{\partial y^2} \right)^2 dy \quad (102)$$

and with Eq. (100) can be written as

$$E_s = EI \left[\frac{12}{\ell^3} (v_2 - v_1)^2 + \frac{4}{\ell} (\theta_2^2 + \theta_1^2 + \theta_1 \theta_2) + \frac{12}{\ell^2} (v_1 \theta_1 + v_1 \theta_2 - v_2 \theta_1 - v_2 \theta_2) \right] \quad (103)$$

References

- [1] W. N. Sharpe, Murray Lecture - Tensile testing at the micrometer scale: opportunities in experimental mechanics, *Exp. Mech.* **43** [3] (2003) 228-237.
- [2] V. T. Srikar and S. M. Spearing, A critical review of microscale mechanical testing methods used in the design of microelectromechanical systems, *Exp. Mech.* **43** [3] (2003) 238-247.
- [3] M. A. Haque and M. T. A. Saif, A review of MEMS-Based microscale and nanoscale tensile and bending testing, *Exp. Mech.* **43** [3] (2003) 248-255.
- [4] W. G. Knauss, I. Chasiotis and Y. Huang, Mechanical measurements at the micron and nanometer scales, *Mechanics of Materials* **35** (2003) 217-231.
- [5] D. T. Read and J. W. Dally, A new method for measuring the strength and ductility of thin films, *J. Mater. Res.* **8** [7] (1993) 1542-1549.
- [6] S. Greek, F. Ericson, S. Johansson and J. Schweitz, In-situ tensile strength measurement and Weibull analysis of thick film and thin film micromachined polysilicon structures, *Thin Solid Films* **292** (1997) 247-254.
- [7] M. Gad-El-Hak, *The MEMS Handbook*, (CRC Press, 2002).
- [8] I. Chasiotis and W. G. Knauss, A new microtensile tester for the study of MEMS materials with the aid of atomic force microscopy, *Exp. Mech.* **42** [1] (2002) 51-57.
- [9] C. A. Sciammarella, Overview of optical techniques that measure displacements: Murray lecture, *Exp. Mech.* **43** [1] (2003) 1-19.
- [10] T. P. Weihs, S. Hong, J. C. Bravman and W. D. Nix, Mechanical deflection of cantilever micro-beams: a new technique for testing the mechanical properties of thin films, *J. Mater. Res.* **3** [5] (1988) 931-942.

- [11] H. D. Espinosa, B. C. Prorok and M. Fischer, A methodology for determining mechanical properties of freestanding thin films and MEMS materials, *Journal of the mechanics and physics of solids* **51** (2003) 47-67.
- [12] P. Ladevèze, *Comparaison de modèles de milieux continus*, (these d'Etat, Universite Paris 6, 1975).
- [13] R. V. Kohn and B. D. Lowe, A Variational Method for Parameter Identification, *Math. Mod. Num. Ana.* **22** [1] (1988) 119-158.
- [14] J. E. Mottershead and M. I. Friswell, Model updating in structural dynamics: a survey, *Journal of Sound and Vibration* **167** [2] (1993) 347-375.
- [15] G. Geymonat, F. Hild and S. Pagano, Identification of elastic parameters by displacement field measurement, *C. R. Mecanique* **330** (2002) 403-408.
- [16] S. Calloch, D. Dureisseix and F. Hild, Identification de modèles de comportement de matériaux solides : utilisation d'essais et de calculs, *Technologies et Formations* **100** (2002) 36-41.
- [17] M. Grediac, Principe des travaux virtuels et identification, *C. R. Acad Sci. Paris* **309** [Serie II] (1989) 1-5.
- [18] M. Grediac, E. Toussaint and F. Pierron, Special virtual fields for the direct determination of material parameter with the virtual fields method. 1- Principle and definition, *Int. J. SolidsStruct.* **39** (2002) 2691-2705.
- [19] H. D. Bui, Sur quelques problèmes inverses élastiques en mécanique de l'endommagement, *Proceedings 2e Colloque national de calcul des structures*, (Hermes, Paris (France), 1995), 25-35.
- [20] M. Bonnet and A. Constantinescu, Inverse problems in elasticity, *Inverse problems* **21** (2005) 1-50.

- [21] M. Hori, Inverse analysis method to find local constitutive relations, *Mechanics of Materials* **35** (2002) 1089-1105.
- [22] D. Claire, F. Hild and S. Roux, Identification of damage fields using kinematic measurements, *C. R. Mecanique* **330** (2002) 729-734.
- [23] P. E. Barbone and N. H. Gokhale, Elastic modulus imaging: on the uniqueness and nonuniqueness of the elastography inverse problem in two dimensions, *Inverse problems* **20** (2004) 283-296.
- [24] D. Lesnic, Retrieving the flexural rigidity of a beam from deflection measurements, *Proceedings 3rd Int. Conference on Inverse Problems in Engineering*, (ASME, 1999)
- [25] S. P. Timoshenko and J. N. Goodier, *Theory of Elasticity*, (McGraw-Hill (3rd edition), New York (USA), 1970).
- [26] K. T. Kavanagh and R. W. Clough, Finite element applications in the characterization of elastic solids, *Int. J. SolidsStruct.* **7** (1971) 11-23.
- [27] W. H. Press, S. A. Teukolsky, W. T. Vetterling and B. P. Flannery, *Numerical Recipes in C++*, (Cambridge University Press, Cambridge (UK), 2002).
- [28] Demmel J. and Veselic K., Jacobi's method is more accurate than QR. *SIAM J. Sci. Stat. Comput.*, 11, p. 1204-1246, 1992.
- [29] F. Amiot and J.P. Roger, Nomarski imaging interferometry to measure the displacement field of MEMS, *Applied Optics* **45** (2006) 7800-7810.
- [30] A.M. Mathai, *Jacobians of matrix transformations and functions of matrix argument*, World Scientific Publishers, 1997.

List of Tables

- 1 Value of the acceptable noise/signal ratio for a given root-mean-square error on the stiffness and a given discretization level. 45
- 2 Values of the β parameter with 2 elements (β and w_r are dimensionless). 46

Table 1

Value of the acceptable noise/signal ratio for a given root-mean-square error on the stiffness and a given discretization level.

| | $\alpha = 1$ | $\alpha = 2$ | $\alpha = 3$ |
|-------------------------------------|--------------------|----------------------|----------------------|
| $\sqrt{\eta(\mathbf{D})} = 10^{-2}$ | 6×10^{-3} | 4.2×10^{-5} | 4.6×10^{-6} |
| $\sqrt{\eta(\mathbf{D})} = 10^{-3}$ | 5×10^{-4} | 4.2×10^{-6} | 4.5×10^{-7} |
| $\sqrt{\eta(\mathbf{D})} = 10^{-4}$ | 5×10^{-5} | 5×10^{-7} | 4.6×10^{-8} |

Table 2

Values of the β parameter with 2 elements (β and w_r are dimensionless).

| $\delta \mathbf{U}_{sol}^t \mathbf{U}_p$ | β | w_r (a.u.) |
|--|---------|----------------------|
| 0 | 0 | 2.8 |
| 6×10^{-6} | -1.45 | 4×10^{-14} |
| 0 | -1.38 | 4×10^{-2} |
| 0 | -1.53 | 3.8×10^{-2} |

List of Figures

| | | |
|---|---|----|
| 1 | Description of the discretized test beam and applied loading. | 49 |
| 2 | Elastic property field \mathbf{C} and shape of the tested beam. | 50 |
| 3 | a) Errors $\eta(D)$ and $\eta(F)$ vs. amplitude of the added white noise for different discretization levels. b) Global indicator w_r vs. errors $\eta(D)$ for different discretization levels. | 51 |
| 4 | Norm of the residual equilibrium gap in the vicinity of the solution. | 52 |
| 5 | a) Value of the kinematic noise criterion in the vicinity of the solution. b) Plot of the probability density for β . | 52 |
| 6 | a) General SEM view of the used cantilevers. b) SEM view of the base under the cantilever. | 53 |
| 7 | Schematic view of the electrostatic loading device. | 53 |
| 8 | Description of the modified discretized beam with an unknown couple. | 54 |
| 9 | Typical measured optical phase field during the electrostatic test. | 54 |

| | | |
|----|---|----|
| 10 | a) Contribution of each element to the error estimator w_r when the identification is performed with $\beta = 0$. b) Measured displacement field (dots) and the best SA displacement field (solid line) obtained with $\beta = 0$ (the rigid body motion is chosen to minimize $\ \mathbf{U}_{SA} - \mathbf{U}_m\ _{KA}$) | 55 |
| 11 | a) Measured displacement field. b) Results of the identification with 2 elements and a pure pressure field. c) Results of the identification with an extra (identified) nodal couple acting on the cantilever. | 56 |
| 12 | Plot of the probability density for β for the analyzed experimental data. | 57 |
| 13 | Measured (dots) and SA (solid line) displacement fields for the identified modeling (the rigid body motion is chosen to minimize $\ \mathbf{U}_{SA} - \mathbf{U}_m\ _{KA}$) | 58 |
| 14 | Parameters and nodal displacements used to describe the displacement field. | 58 |

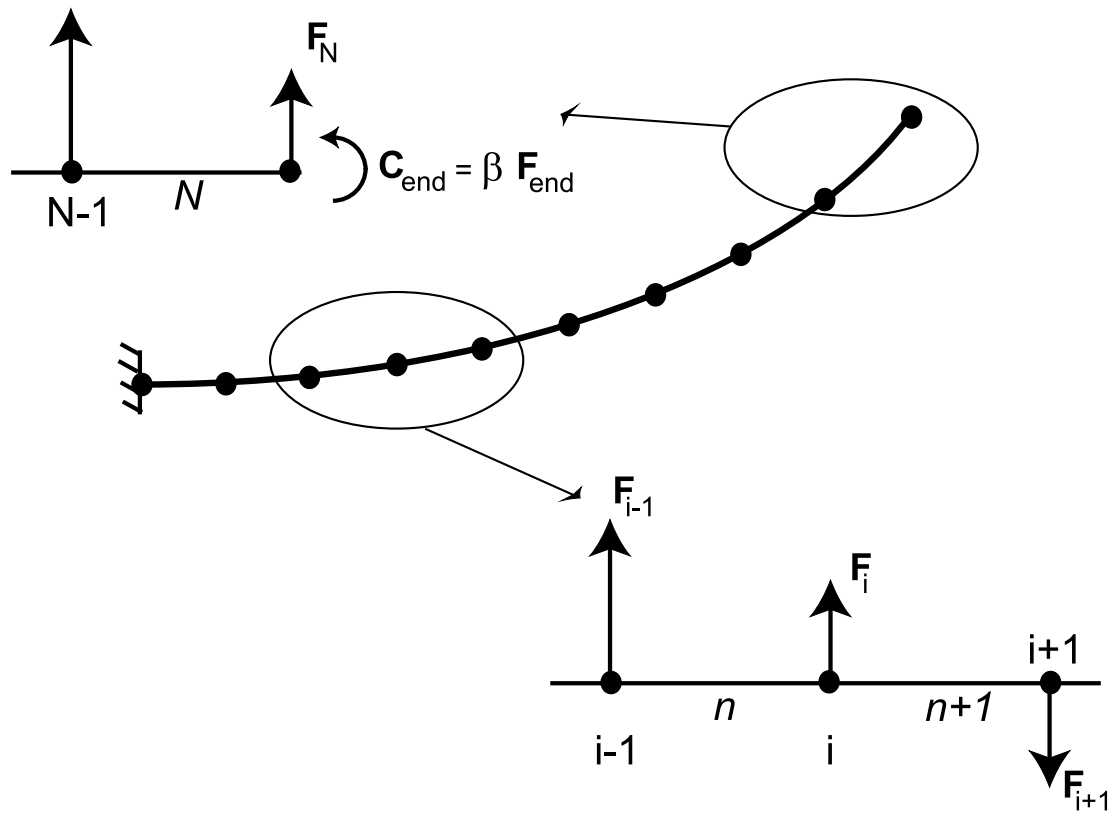


Fig. 1. Description of the discretized test beam and applied loading.

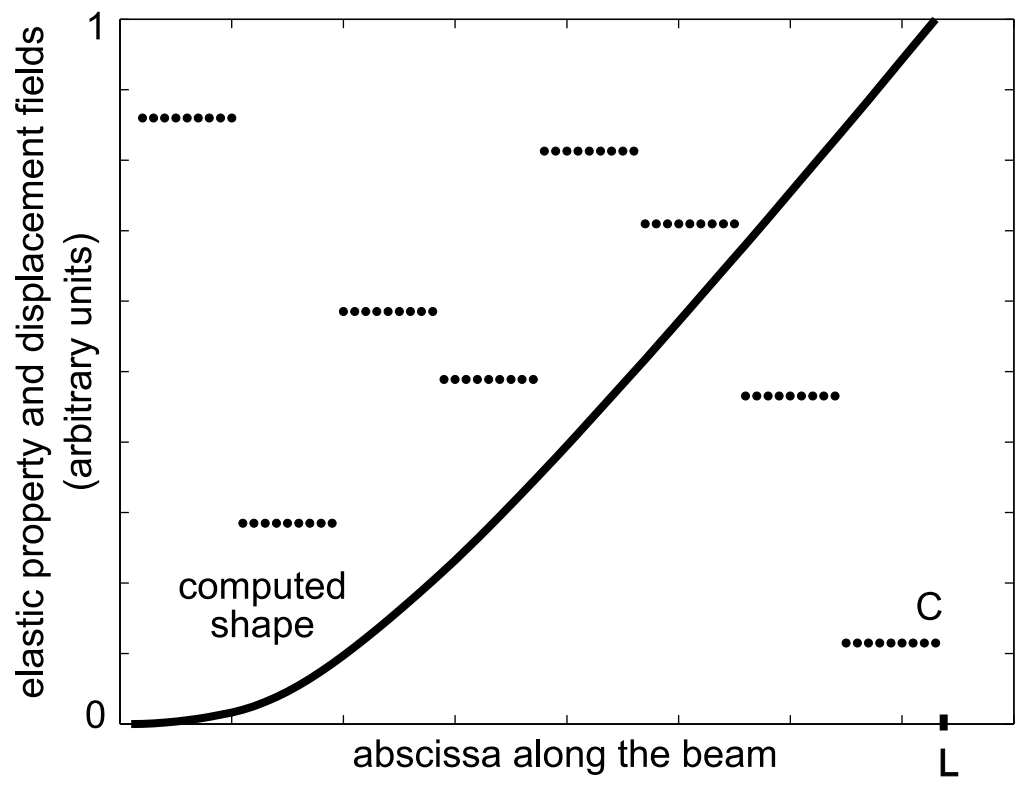


Fig. 2. Elastic property field C and shape of the tested beam.

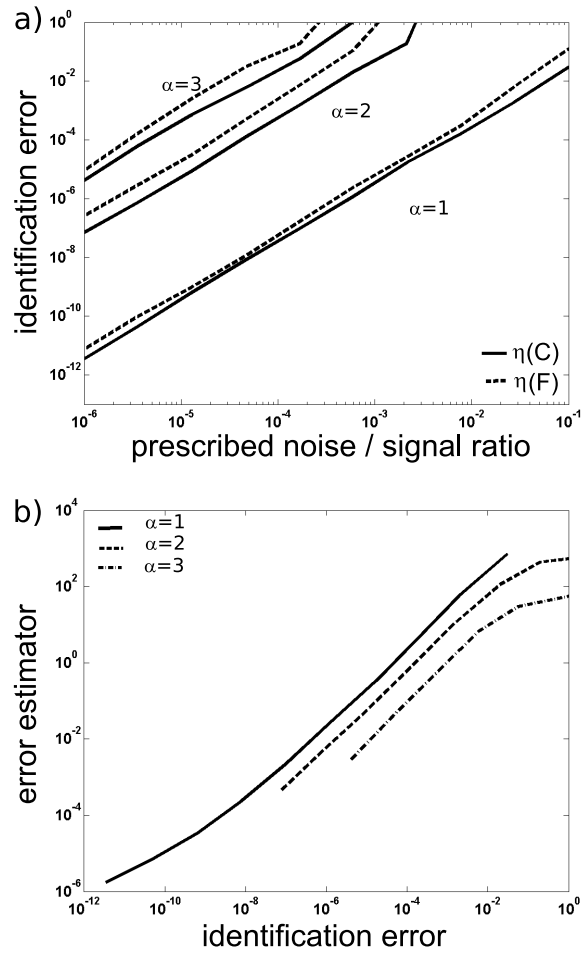


Fig. 3. a) Errors $\eta(D)$ and $\eta(F)$ vs. amplitude of the added white noise for different discretization levels. b) Global indicator w_r vs. errors $\eta(D)$ for different discretization levels.

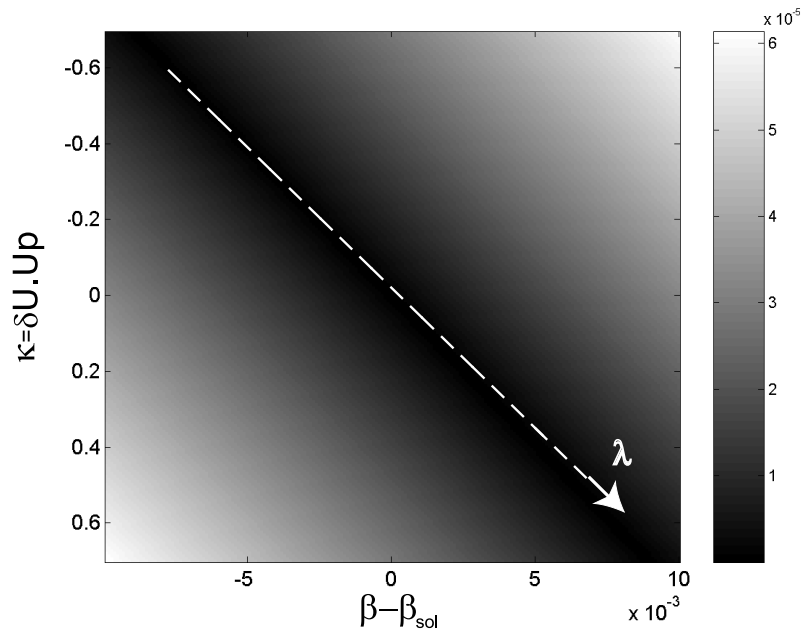


Fig. 4. Norm of the residual equilibrium gap in the vicinity of the solution.

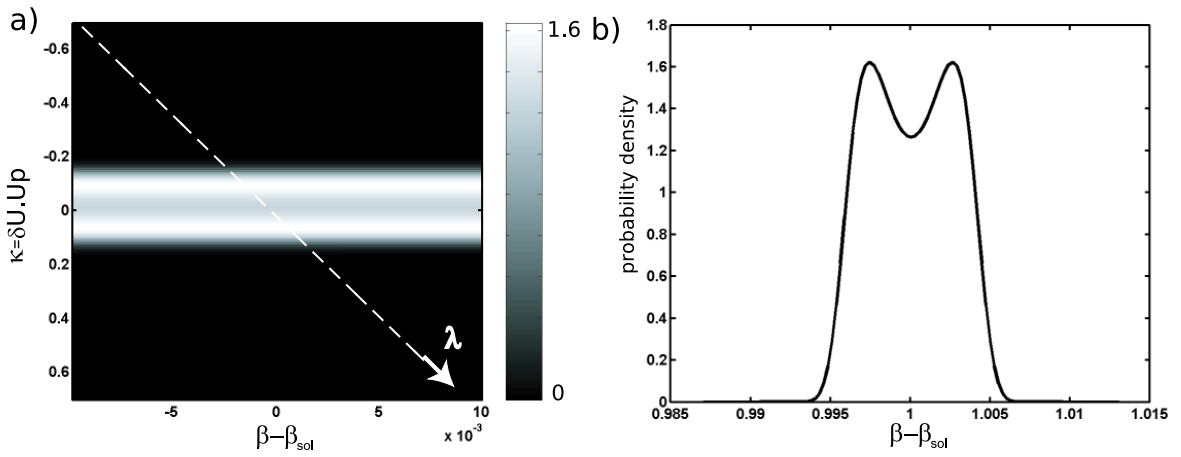


Fig. 5. a) Value of the kinematic noise criterion in the vicinity of the solution. b) Plot of the probability density for β .

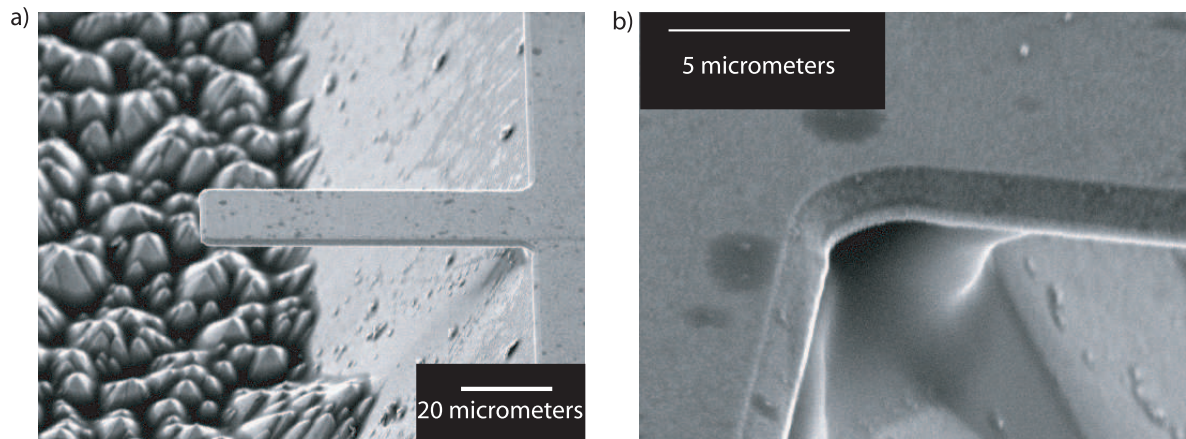


Fig. 6. a) General SEM view of the used cantilevers. b) SEM view of the base under the cantilever.

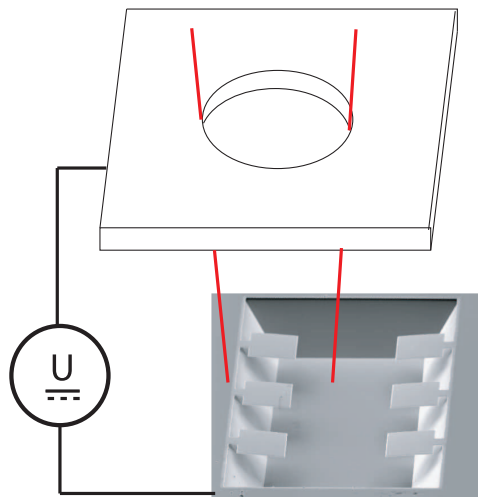


Fig. 7. Schematic view of the electrostatic loading device.

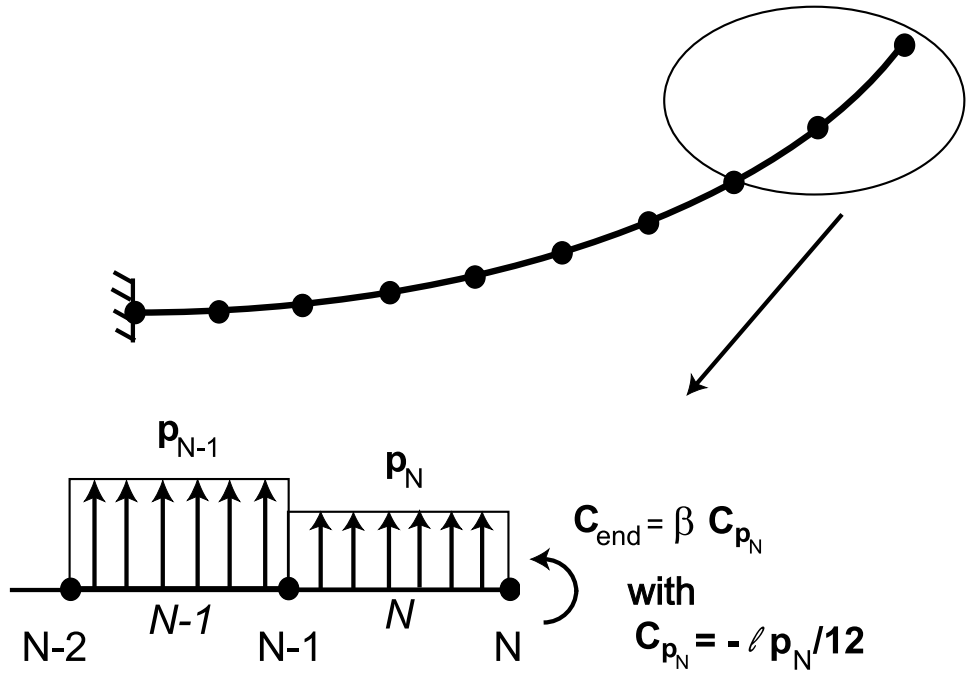


Fig. 8. Description of the modified discretized beam with an unknown couple.

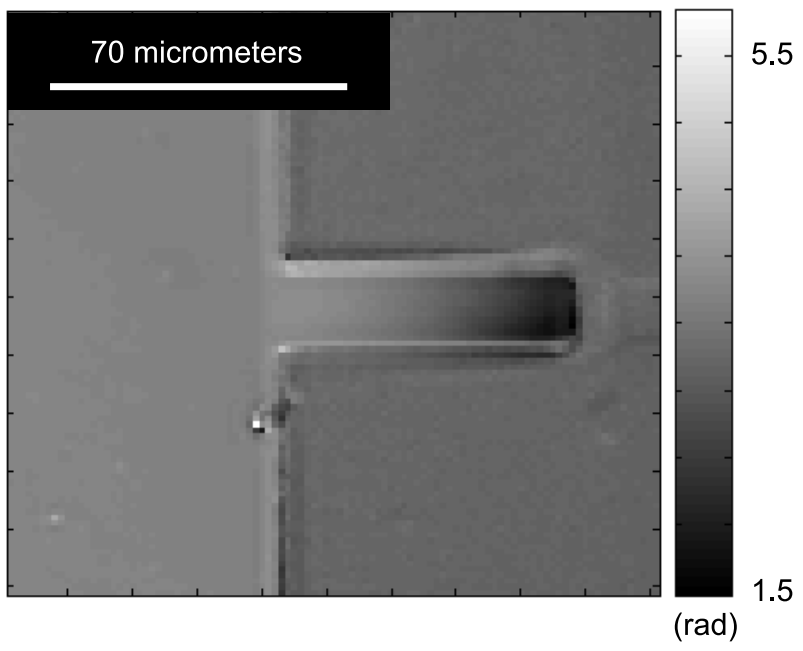


Fig. 9. Typical measured optical phase field during the electrostatic test.

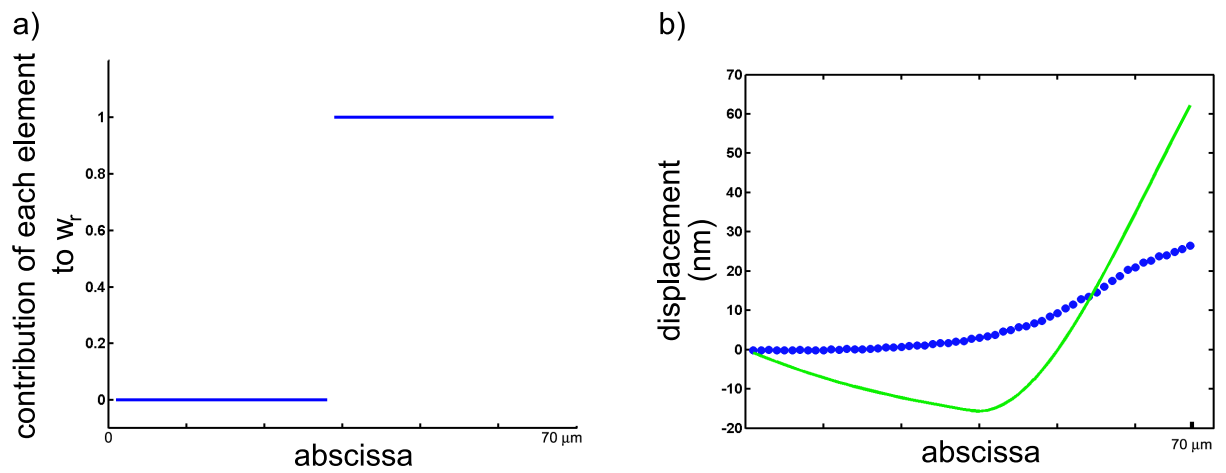


Fig. 10. a) Contribution of each element to the error estimator w_r when the identification is performed with $\beta = 0$. b) Measured displacement field (dots) and the best SA displacement field (solid line) obtained with $\beta = 0$ (the rigid body motion is chosen to minimize $\|\mathbf{U}_{SA} - \mathbf{U}_m\|_{KA}$)

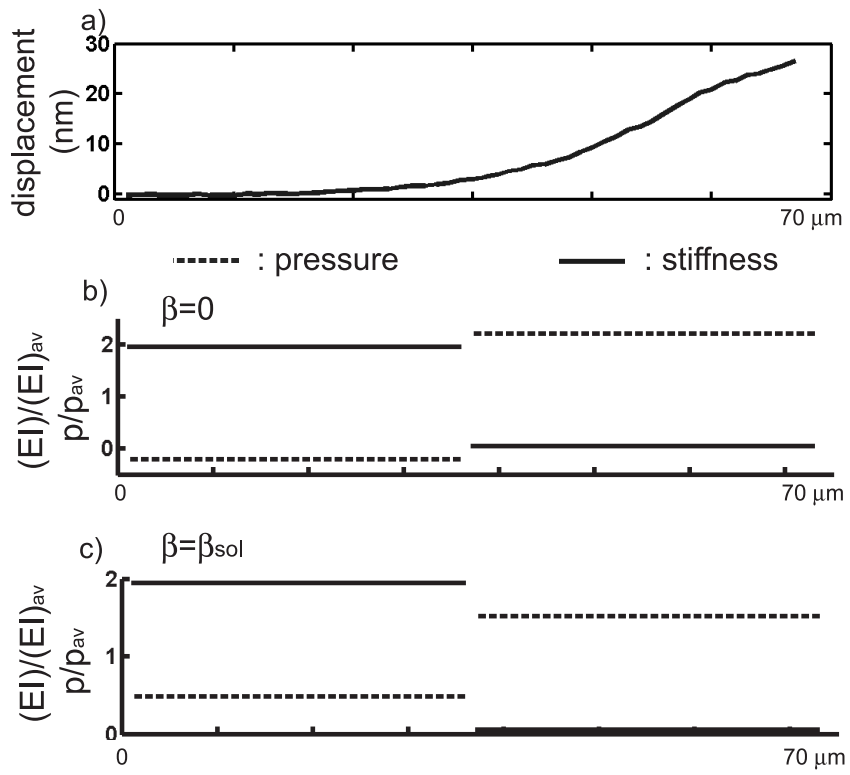


Fig. 11. a) Measured displacement field. b) Results of the identification with 2 elements and a pure pressure field. c) Results of the identification with an extra (identified) nodal couple acting on the cantilever.

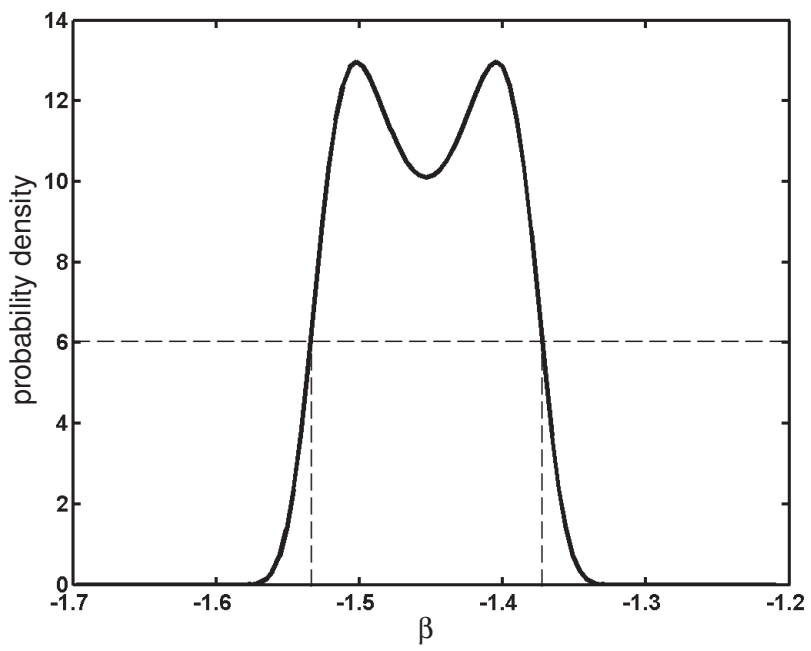


Fig. 12. Plot of the probability density for β for the analyzed experimental data.

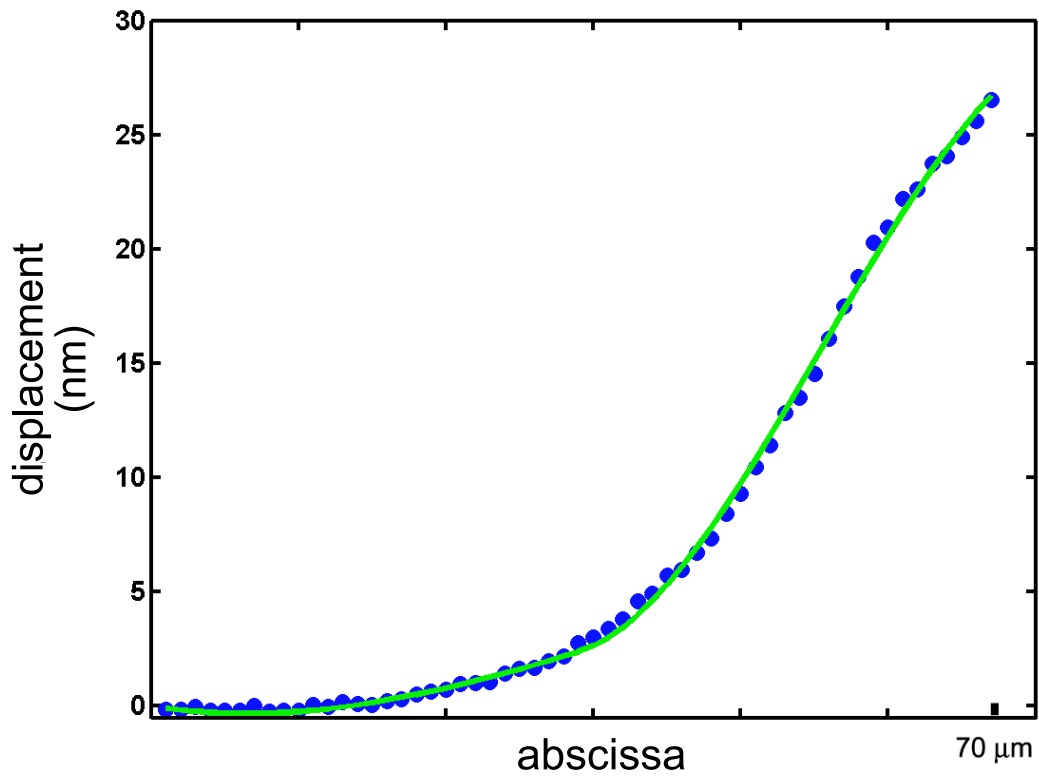


Fig. 13. Measured (dots) and SA (solid line) displacement fields for the identified modeling (the rigid body motion is chosen to minimize $\|\mathbf{U}_{SA} - \mathbf{U}_m\|_{KA}$)

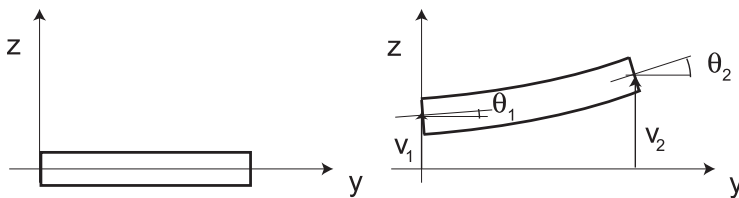


Fig. 14. Parameters and nodal displacements used to describe the displacement field.